JOURNAL OF TISSUE ENGINEERING AND REGENERATIVE MEDICINE
J Tissue Eng Regen Med 2017; **11**: 3508–3522.
Published online 29 March 2017 in Wiley Online Library (wileyonlinelibrary.com) **DOI:** 10.1002/term.2263

RESEARCH ARTICLE

The geometrical shape of mesenchymal stromal cells measured by quantitative shape descriptors is determined by the stiffness of the biomaterial and by cyclic tensile forces

Tatiana Uynuk-Ool[1†], Miriam Rothdiener[1†], Brandan Walters[2], Miriam Hegemann[3], Julian Palm[1], Phong Nguyen[1], Tanja Seeger[4], Ulrich Stöckle[5], Jan P. Stegemann[2], Wilhelm K. Aicher[3], Bodo Kurz[6], Melanie L. Hart[1], Gerd Klein[4] and Bernd Rolauffs[7*]

[1]*Siegfried Weller Institute for Trauma Research, BG Trauma Clinic Tübingen, University of Tübingen, Tübingen, Germany*
[2]*Department of Biomedical Engineering, University of Michigan, Ann Arbor, MI, United States*
[3]*Department of Urology, University of Tübingen, Tübingen, Germany*
[4]*University Medical Clinic, Department II, Centre for Medical Research, University of Tübingen, Tübingen, Germany*
[5]*Clinic for Trauma and Restorative Surgery, BG Trauma Clinic Tübingen, University of Tübingen, Tübingen, Germany*
[6]*Department of Anatomy, Christian-Albrechts-University, Kiel, Germany*
[7]*Department of Orthopedics and Trauma Surgery, Medical Center - Albert-Ludwigs-University of Freiburg, Faculty of Medicine, Albert-Ludwigs-University of Freiburg, Freiburg, Germany*

Abstract

Controlling mesenchymal stromal cell (MSC) shape is a novel method for investigating and directing MSC behaviour *in vitro*. it was hypothesized that specifigc MSC shapes can be generated by using stiffness-defined biomaterial surfaces and by applying cyclic tensile forces. Biomaterials used were thin and thick silicone sheets, fibronectin coating, and compacted collagen type I sheets. The MSC morphology was quantified by shape descriptors describing dimensions and membrane protrusions. Nanoscale stiffness was measured by atomic force microscopy and the expression of smooth muscle cell (SMC) marker genes (*ACTA2, TAGLN, CNN1*) by quantitative reverse-transcription polymerase chain reaction. Cyclic stretch was applied with 2.5% or 5% amplitudes. Attachment to biomaterials with a higher stiffness yielded more elongated MSCs with fewer membrane protrusions compared with biomaterials with a lower stiffness. For cyclic stretch, compacted collagen sheets were selected, which were associated with the most elongated MSC shape across all investigated biomaterials. As expected, cyclic stretch elongated MSCs during stretch. One hour after cessation of stretch, however, MSC shape was rounder again, suggesting loss of stretch-induced shape. Different shape descriptor values obtained by different stretch regimes correlated significantly with the expression levels of SMC marker genes. Values of approximately 0.4 for roundness and 3.4 for aspect ratio were critical for the highest expression levels of *ACTA2* and *CNN1*. Thus, specific shape descriptor values, which can be generated using biomaterial-associated stiffness and tensile forces, can serve as a template for the induction of specific gene expression levels in MSC.

Received 9 September 2015; Revised 15 April 2016; Accepted 3 July 2016

Keywords **mesenchymal stromal cell; MSC; shape; shape descriptor; compacted collagen; cyclic stretch; roundness; aspect ratio; circularity; solidity; nanoscale stiffness; myogenic differentiation; biomaterial; silicone**

1. Introduction

The shape of cells is a fundamental signal of proliferation (Singhvi et al., 1994), a potent regulator of cell growth and physiology, and is adapted for specific functions (Folkman and Moscona, 1978). During embryonic development and tissue regeneration, many events are initiated to change stem cell shape, and this change in shape can influence tissue structure and function (Manasek et al., 1972; Yang et al., 1999). Mesenchymal stromal cells (MSCs) can differentiate *in vitro* into cell types of mesodermal origin including osteogenic, chondrogenic, adipogenic and myogenic lineages (Caplan, 2007; Aicher et al., 2011; Klein et al., 2015). To control MSC differentiation via controlling cellular shape, previous studies have generated dynamically elongated shapes using cyclic tensile forces (Park et al., 2004; Maul et al., 2011). In addition, specific shape geometries were engineered using adhesive micropatterned surfaces (McBeath et al., 2004; Kilian et al., 2010) and multi-perforated polycarbonate membranes (Yang et al., 1999). Thus, controlling MSC shape is an important method for investigating, understanding, and controlling MSC behaviour *in vitro*.

The shape of individual cells is based on the balance between external biomechanical forces and internal cellular forces, and the level of internal forces is proportional to the elastic material properties of the surrounding

**Correspondence to: Bernd Rolauffs, Department of Orthopedics and Trauma Surgery, Medical Center - Albert-Ludwigs-University of Freiburg, Faculty of Medicine, Albert-Ludwigs-University of Freiburg, Engesserstraße 4, 79108 Freiburg, Germany. E-mail: berndrolauffs@googlemail.com*
†Shared first authorship.

extracellular matrix (Sun et al., 2012). This suggests that cell shape can be controlled through both matrix elasticity and biomechanical forces. It was therefore hypothesized that specific MSC shapes can be generated as a function of the biomaterials chosen and the nanoscale stiffness associated with these biomaterials. Accordingly, the shapes of human bone-marrow derived MSCs that adhered to different biomaterials with similar stiffnesses vs. similar biomaterial types with different stiffnesses were compared to determine whether specific baseline shapes could be generated by altering biomaterial substrate properties. For this purpose, compressed collagen sheets (Rothdiener et al., 2016) and uncoated and fibronectin-coated silicone sheets were used. The MSC shape was described using a semi-automated high-throughput method for calculating quantitative shape descriptors.

With cell shape being affected by the balance between external and internally generated forces, it was theorized that changes in external force would prompt a subsequent change in shape. It was also hypothesized that the application of tensile forces results in MSC elongation during cyclic stretch, and that the effects on MSC elongation are diminished upon cessation of stretch. Hence, over time, the MSC shape may revert towards its original biomaterial-dictated state much like an elastic rubber band released from tension. This was tested by comparing the shape of MSCs that adhered to cyclically stretched compressed collagen sheets with that of MSCs that adhered to non-stretched control sheets. Importantly, this setup established a system of two competing cues: dynamic effects on MSC shape through cyclic stretch and static effects on shape through the stiffness-defined biomaterial. This allowed one to answer whether dynamic cues on shape can potentially overpower static cues, or vice versa. Because elongated MSC morphologies are associated with increased expression of smooth muscle markers (Yang et al., 1999; Maul et al., 2011), and it has been shown that biomechanical forces can increase MSC differentiation towards a smooth muscle cell (SMC) phenotype (Hamilton et al., 2004; Nieponice et al., 2007; Maul et al., 2011), the present study investigated how the generated MSC shapes correlated with MSC differentiation towards a SMC phenotype. The ability to understand and control MSC shape would be an important tool in directing the behaviour of these cells and would advance the fields of biomaterials, biomechanics, and tissue engineering.

2. Materials and methods

2.1. Biomaterials

2.1.1. Compressed collagen type I sheets

Compressed collagen was produced with Amedrix (Esslingen, Germany). Collagen type I fibres were isolated from de-skinned rat tails, washed in acetic acid for 24 h, purified, and lyophilized. Rat collagen type I hydrogels with an initial collagen concentration of 8 mg/ml were generated and mechanically compressed from initial thicknesses of 10 mm and 20 mm down to 1-mm thick sheets within a custom-made polycarbonate chamber (20.0 × 2.7 × 5.0 cm) with a porous polytetrafluoroethylene (PTFE) bottom. The PTFE pore size was 100 μm to allow water effusion during compression. For hydrogel compression within the chamber, weights were used to generate compressed collagen with final concentrations of 80 mg/ml and 160 mg/ml. Sheets at 80 mg/ml were generated with a weight of 2 kg applied for 2 h, 4 kg applied overnight, 9.5 kg for 8 h, and 27 kg overnight (total time of compression 34 h). For 160 mg/ml sheets, the final compression step applied 27 kg for 30 h (total time of compression 52 h).

2.1.2. Silicone sheets and silicone coating procedures

Non-reinforced vulcanized matt silicone sheets with thicknesses of 127 μm (termed 'thin') and 762 μm (termed 'thick') were obtained from Specialty Manufacturing (No. 70P001-200-005 and 70P001-200-030, both 40durometer-Shore-A; Saginaw, Michigan, USA). Thick silicone sheets were coated with fibronectin from bovine plasma (F1141; Sigma-Aldrich, Seinheim, Germany) diluted in PBS (12.5 μg/ml). Silicone sheets (2 × 1 cm) were covered with 700 μl coating substrate in 12-well culture plates for 24 h (room temperature), washed with 0.05% Tween 20 in 2 ml phosphate-buffered saline (PBS), and washed three times with 2 ml PBS.

2.2. Atomic force microscopy

Atomic force microscopy (AFM) was performed to characterize the nanoscale stiffness of the biomaterial surfaces. Microspheres (Polybead Polystyrene 25.0 Micron Microspheres; Polysciences, Eppelheim, Germany) were attached to a tipless cantilever (All-in-One-cantilever D, 40 N/m nominal spring constant; Budget Sensors, Sofia, Bulgaria) using the M-Bond 610–1 adhesive single kit according to the manufacturer's instructions (Micro-Measurements, Vishay Precision Group, Wendell, USA). The cantilever of the atomic force microscope (CellHesion 200; JPK Instruments, Berlin, Germany) was calibrated on the extend curve and its spring constant was determined using the thermal noise method of the software (JPK Instruments). Samples were measured with a maximum force of 800 nN and an extend speed of 5 μm/sec in triplicates at three locations for each sheet. The Young's modulus was calculated using the Hertz model fit of the data processing software (JPK Instruments).

2.3. Human bone marrow MSCs

2.3.1. Source

Bone-marrow samples were obtained with institutional approval of the local research ethics committee and with informed consent (reference number 623/2013BO2) from

DOI: 10.1002/term

the proximal femur of patients undergoing total hip replacement (n = 14, age 50–86 years) in the Department of Trauma and Restorative Surgery, BG Trauma Clinic, University of Tübingen.

2.3.2. Isolation, culture and characterization

Bone marrow MSCs were prepared as described previously (Felka et al., 2009). The samples were washed with PBS and centrifuged at 150 ***g*** (10 min, room temperature) and resuspended in PBS. The MSCs were isolated using a Ficoll density gradient fractionation (density 1.077 g/ml, 400 ***g***, 30 min, room temperature; GE Healthcare–Life Sciences, Uppsala, Sweden). The mononuclear cell layer was harvested, washed with PBS and seeded in T75-flasks. MSCs were expanded using good manufacturing practice (GMP)-compliant expansion medium consisting of Dulbecco's Modified Eagle Medium (DMEM, low glucose; Sigma-Aldrich, Hamburg, Germany) including 25 mM hydroxyethyl piperazineethanesulfonic acid (HEPES, 2.4% of total volume; Lonza Group, Basel, Switzerland), 0.2% (1000 IU) heparin (Carl Roth, Karlsruhe, Germany), 5% human plasma (TCS Biosciences, Buckingham, UK), 5% human pooled platelet lysate (10^8 platelets/ml medium; UKT Tübingen, Germany), 1% L-glutamine (Lonza Group), and 1% penicillin–streptomycin solution (Life Technologies, Darmstadt, Germany). After 24 h (37°C, 5% CO_2), medium was replaced to remove non-attached cells and GMP expansion medium was changed twice per week. After 5–7 days, cells were removed with trypsin and reseeded in GMP-expansion medium (passage 1, density 1.5 × 10^5 cells/flask). The expression of MSC cell surface antigens and their adipogenic, osteogenic and chondrogenic differentiation were successfully demonstrated as we have shown previously (Felka et al., 2009; Pilz et al., 2011; Ulrich et al., 2013), and in accordance with the method of Dominici et al. (2006) (data not shown).

2.4. MSCs on biomaterials

2.4.1. Seeding and cell culture

After expansion in GMP-expansion medium, MSCs were seeded at passages 2–5 (density: 5000 MSCs/cm^2) at day 0 onto the biomaterials and in medium consisting of DMEM high glucose (4 g/l; Life Technologies), 10 % FBS (Biochrom, Berlin, Germany), 1% penicillin–streptomycin solution (Life Technologies) and 1% fungicide (Biochrom, Berlin, Germany) at 37°C and 5% CO_2. Upon binding of the MSCs to the different biomaterial surfaces used in the present study, different cellular shapes appeared spontaneously. These were subjected to further investigation.

2.4.2. Sinusoidal cyclic stretch

Compacted collagen sheets (80 mg/ml) were seeded with MSCs at passages 2–5 at day 0 (n = 13 bone marrow samples from n = 8 donors; age range 61–81 years, average age 69.1 years, gender ratio 1:1, seeding density 5000 MSCs/cm^2). They were inserted at day 4 and day 5 into the bioreactor chamber (150 ml medium) of an incubator-housed ElectroForce-5210 BioDynamic Test System (Bose, Eden Prairie, MN, USA), and stretched with displacement-controlled uniaxial cyclic stretch (strain 2.5% and 5%, 60 min, f = 1 Hz) for 1 h on day 4 and on day 5. Non-stretched MSCs served as controls. Each individual experiment consisted of six compacted collagen sheets: two controls, two sheets 1 h after completion of 2.5% stretch and two sheets after 5% stretch. Half of the first sheet was used for quantitative reverse-transcription polymerase chain reaction (qRT-PCR), and the second half was used for fluorescence microscopy. To visualize MSCs during stretch, sheets were manually stretched on top of a microscope slide to a previously marked position (5% stretch) and fixed to the slide with two clamps for fluorescence microscopy.

2.4.3. Fluorescence microscopy

The cellular shapes that were generated by the MSCs while attached to the various biomaterial surfaces were visualized by fluorescence microscopy. Cells were stained with the fluorescent dye calcein (Cell Viability Imaging Kit; Roche, Mannheim, Germany) according to the manufacturer's protocol to assess MSC shapes (see below). Adherent MSCs were digitally recorded in a top-down view (Zeiss LSM-510, AxioVison-4.8, Zeiss, Oberkochen, Germany) according to (Rolauffs et al., 2010, 2011). Image mosaics consisting of 10 × 10 tiles (12 633 × 9429 pixels corresponding to 8211.45 × 6,128.85 μm) were reconstructed (Module MosaiX) for cyclically stretched sheets and controls. For manually stretched sheets, mosaics of 17 629 × 7 564 pixels (11 458.85 × 4916.6 μm) were reconstructed. The numbers of stained nuclei were counted using ImageJ (NIH, Bethesda, MD, USA).

2.4.4. MSC shape descriptors

Calcein-stained MSCs were recorded using a Zeiss LSM-510 digital microscope and the images were processed to reconstruct image mosaics. Using ImageJ, the four shape descriptors – roundness ($4 \times \text{area}/\pi \times \text{major\_axis\_length}^2$), aspect ratio (major_axis_length/minor_axis_length), circularity ($4\pi \times \text{area}/\text{perimeter}^2$) and solidity (area/convex_area) – and the total number of cells/normalized area were calculated individually for each recorded cell. The user input was to set a manual threshold and the scale, which was 1.695 pixels/1 μm. A median filter with a radius of 2 pixels was then applied for image smoothening before automated shape descriptor calculations.

2.4.5. Gene expression (qRT-PCR)

Compressed collagen sheets were digested with Proteinase K (4 min, 55°C; Fermentas/ThermoScientific). mRNA was isolated using the RNA-Extraction-RNeasy-Minikit (Qiagen, Valencia, CA, USA). cDNA was synthesized with the Advantage RT-for-PCR Kit (Clontech,

USA). Quantitative RT-PCR was performed with the LightCycler-480 SybrGreen Master and LightCycler-480 Probes Master using a LightCycler 480 and 96-multiwell plates (Roche). Gene expression levels of alpha-smooth-muscle-actin (*ACTA2*), transgelin (*TAGLN*), calponin (*CNN1*), peptidylproplyl-isomerase-A (*PPIA*) and human glycerinaldehyde-3-phosphate-dehydrogenase (*GAPDH*) were determined according to MIQE guidelines (Bustin et al., 2009) (reference genes: *PPIA*, *GAPDH*). As positive controls and calibrator samples human bladder-derived smooth muscle cells (HBdSMC; Promocell, Heidelberg, Germany) were used. The oligonucleotide primers were TTG CCT GAT GGG CAA GTG AT (forward primer sequence) and TAC ATA GTG GTG CCC CCT GA (reverse primer sequence) for *ACTA2*, AGA TGG CAT CAT TCT TTG CGA and GCT GGT GCC AAT TTT GGG TT for *CNN1*, CTC TGC TCC TCC TGT TCG and ACG ACC AAA TCC GTT GAC TC for *GAPDH*, and TTC ATC TGC ACT GCC AAG AC and TCG AGT TGT CCA CAG TCA GC for *PPIA*. For *TAGLN*, the Qiagen assay Hs_TAGLN_2_SG (QT01678516) was used. For *TAGLN* and *PPIA,* SybrGreen (Roche), and for *ACTA2*, *CNN1* and *GAPDH* the Roche Universal Probe Library Probes N58 (*ACTA2*), N71 (*CNN1*) and N60 (*GAPDH*) were used. To confirm gene expression changes on protein level, western blotting was performed (see the Supplementary material online).

2.5. Statistical analyses

All data are presented as mean ± SEM except when box plots were chosen for data presentation. The box plots give the median, 25th and 75th as well as the 10th and 90th percentiles and outlying points. Calculations were performed with Microsoft Excel 2010 and SigmaPlot-11.0.0.77 (Systat, Chicago, MI, USA). Data were analysed for normality (Kolmogorov–Smirnov test). To compare two groups, normally distributed data were subjected to the Student's *t*-test and non-normal data were subjected to the Mann–Whitney rank sum test. More than two groups were compared using analysis of variance (ANOVA) and appropriate *post-hoc* tests. Correlation analyses were performed using Spearman rank-order correlation tests (non-normal data distribution) or Pearson product–moment correlation tests (normal distribution). Differences were considered statistically significant (*) at $P < 0.05$.

3. Results

3.1. Shape descriptors for quantifying MSC morphology

Figure 1a shows representative images of calcein-stained MSCs that were recorded digitally, illustrating the wide range of MSC shapes encountered throughout the present study. Using these images, the parameter roundness were quantitatively calculated (see below, section 3.2) for each individual cell and sorted the depicted MSCs according to their corresponding roundness values. In addition, *in silico* patterns were drawn with Adobe Photoshop and Microsoft PowerPoint, and their shapes were calculated with the four quantitative shape descriptors (roundness, aspect ratio, circularity, and solidity; see below) to demonstrate how these can be used to analyse MSC shape in detail, and how changes in shape can be quantified by these four shape descriptors (Figure 1b,c). Figure 1df is intended to be used by the reader as a reference chart to 'translate' reported shape descriptor values into images.

3.2. Shape descriptors of MSCs adhering to various biomaterials

3.2.1. Shape descriptors of MSCs adhering to similar biomaterial types with different nanoscale stiffnesses

As a first step, the effects of similar biomaterial types with different nanoscale stiffnesses were tested on the four shape descriptors for MSCs that adhered to uncoated thick vs. thin silicone sheets (Figure a–e). Interestingly, all shape descriptors were significantly different for MSCs on thick vs. thin silicone sheets ($P < 0.001$; Figure 2a–d). In particular, MSCs on thick silicone sheets exhibited a significantly lower cellular roundness, higher aspect ratio and circularity, and a lower solidity, indicating a longer MSC morphology with smaller or fewer membrane protrusions, compared with MSCs on thin silicone sheets. To investigate a potential correlation with the nanoscale stiffness of the biomaterials used, the nanoscale stiffness of the biomaterial surfaces were determined by calculating the Young's modulus. For uncoated thick silicone sheets the Young's modulus was 903.2 ± 18.8 kPa. This value was significantly higher than the Young's modulus of uncoated thin silicone sheets ($P < 0.001$), which was 185.8 ± 14.2 kPa (Figure 2e). This suggested that higher nanoscale stiffness was associated with lower cellular roundness, higher aspect ratio and circularity, and a lower solidity.

3.2.2. Shape descriptors of MSCs adhering to different biomaterial types with similar nanoscale stiffnesses

We tested the effects of different biomaterial types with similar nanoscale stiffnesses on the four shape descriptors by comparing MSCs that adhered to uncoated vs. fibronectin-coated thick silicone sheets (Figure 2f–j). There was no significant difference between the four shape descriptors of MSCs on uncoated vs. fibronectin-coated thick silicone sheets (Figure 2f–i). To examine whether this could be explained by similar nanoscale stiffnesses of the two biomaterials, their Young's moduli were determined. There was no significant difference in the nanoscale stiffness of the surfaces of uncoated (903.2 ± 18.8 kPa) vs. fibronectin-coated (811.0 ± 14.7 kPa) thick silicone sheets (Figure 2j). This suggested that the MSC shape descriptor values were

DOI: 10.1002/term

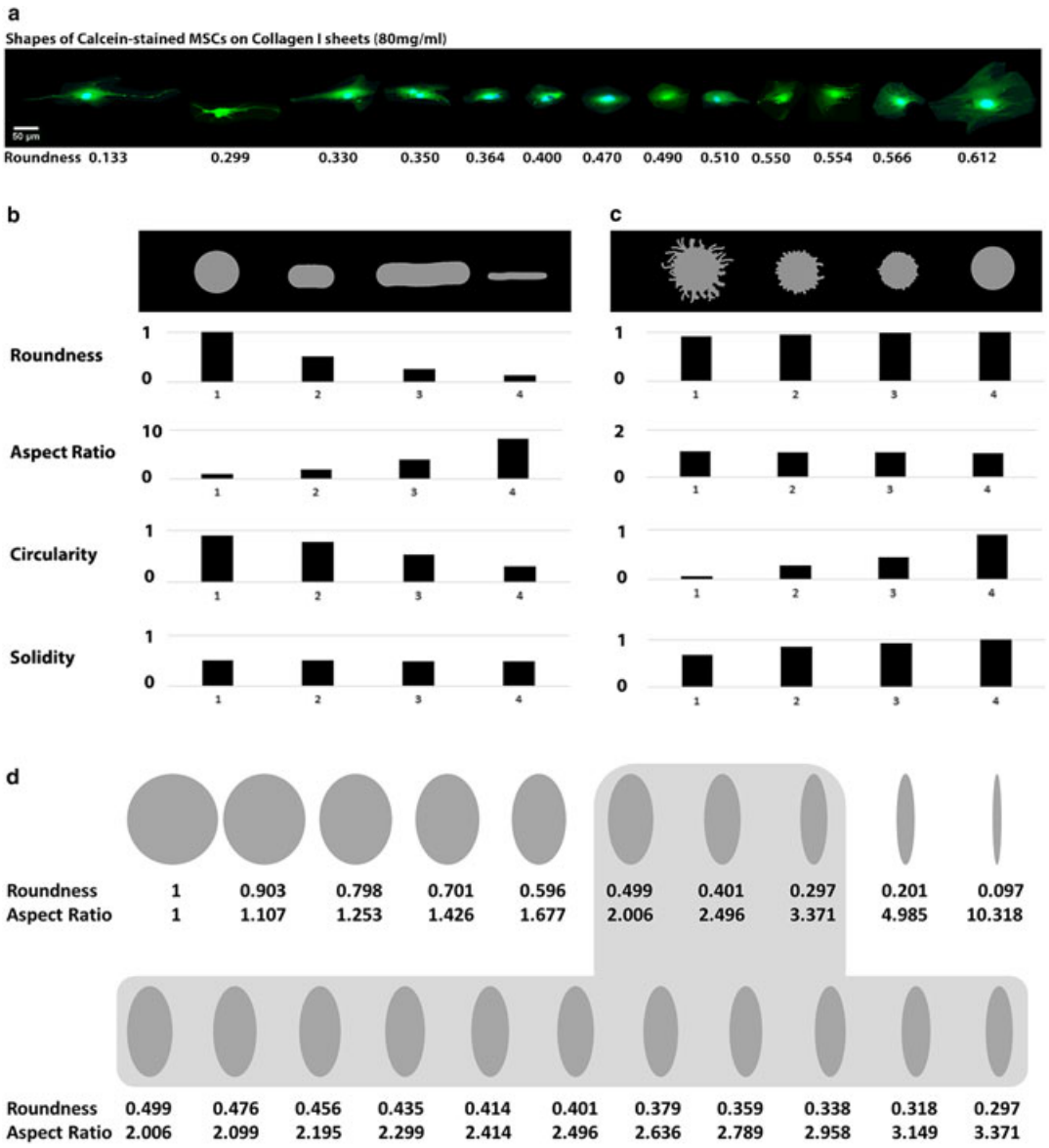

Figure 1. Range of observed mesenchymal stem cell (MSC) shapes and shapes drawn *in silico* to illustrate how changes in shape can be quantified by shape descriptors. Human MSCs that adhered to the surfaces of compacted collagen type I sheets were stained with the fluorescent dye calcein and recorded in a top-down view. The shape descriptor 'roundness' was calculated for each cell individually. (a) Representative images depicting individual MSCs and their associated roundness are given to illustrate the broad range of shapes that was observed in the present study. Bar: 50 µm. (b) A circular shape morphing into an elongated shape is best quantified with the descriptors roundness and aspect ratio. A high value for roundness indicates a round cell, and a high aspect ratio indicates a rather elongated cell. High values for both circularity and solidity indicate the absence of (cellular) protrusions. (c) A circle with a large number of protrusions morphing into a circle without protrusions is best quantified by the descriptors circularity and solidity, while roundness and aspect ratio remain unchanged. (d) Reference chart to 'translate' reported shape descriptor values into images by providing standardized shape changes, analogous to commonly used standard curves. [Colour figure can be viewed at wileyonlinelibrary.com]

comparable on different materials with similar stiffnesses (uncoated and fibronectin-coated silicone), and that selected shape descriptor values were associated with the nanoscale stiffness of the biomaterials used for MSC adherence.

3.2.3. Shape descriptors of MSCs adhering to biomaterials with different collagen type I concentrations

The shape descriptors of MSCs that adhered to compacted collagen sheets produced with different collagen concentrations and the shape descriptors of MSCs on these compacted collagen sheets during days 4 and 5 were assessed (Figure 2k–n). All shape descriptors of MSCs on compacted collagen type I sheets were significantly different, when comparing concentrations of 80 mg/ml vs. 160 mg/ml ($P < 0.001$). In particular, MSCs on 80 mg/ml compacted collagen sheets exhibited a significantly lower roundness (Figure 2k) and a higher aspect ratio (Figure 2l), circularity (Figure 2m) and solidity (Figure 2n, $P < 0.001$), indicating a longer MSC morphology with smaller or less membrane protrusions on 80 mg/ml sheets, compared with MSCs on 160 mg/ml sheets. When assessing the effect of time on 80 mg/ml and 160 mg/ml sheets (Figure 2k–m), the shape descriptors roundness, aspect ratio and circularity were not significantly different on day 4 vs. day 5. In contrast, day 4 solidity was significantly higher than on day 5 ($P < 0.001$; Figure 2n), indicating that only MSC solidity but not the other shape descriptors underwent time-associated

DOI: 10.1002/term

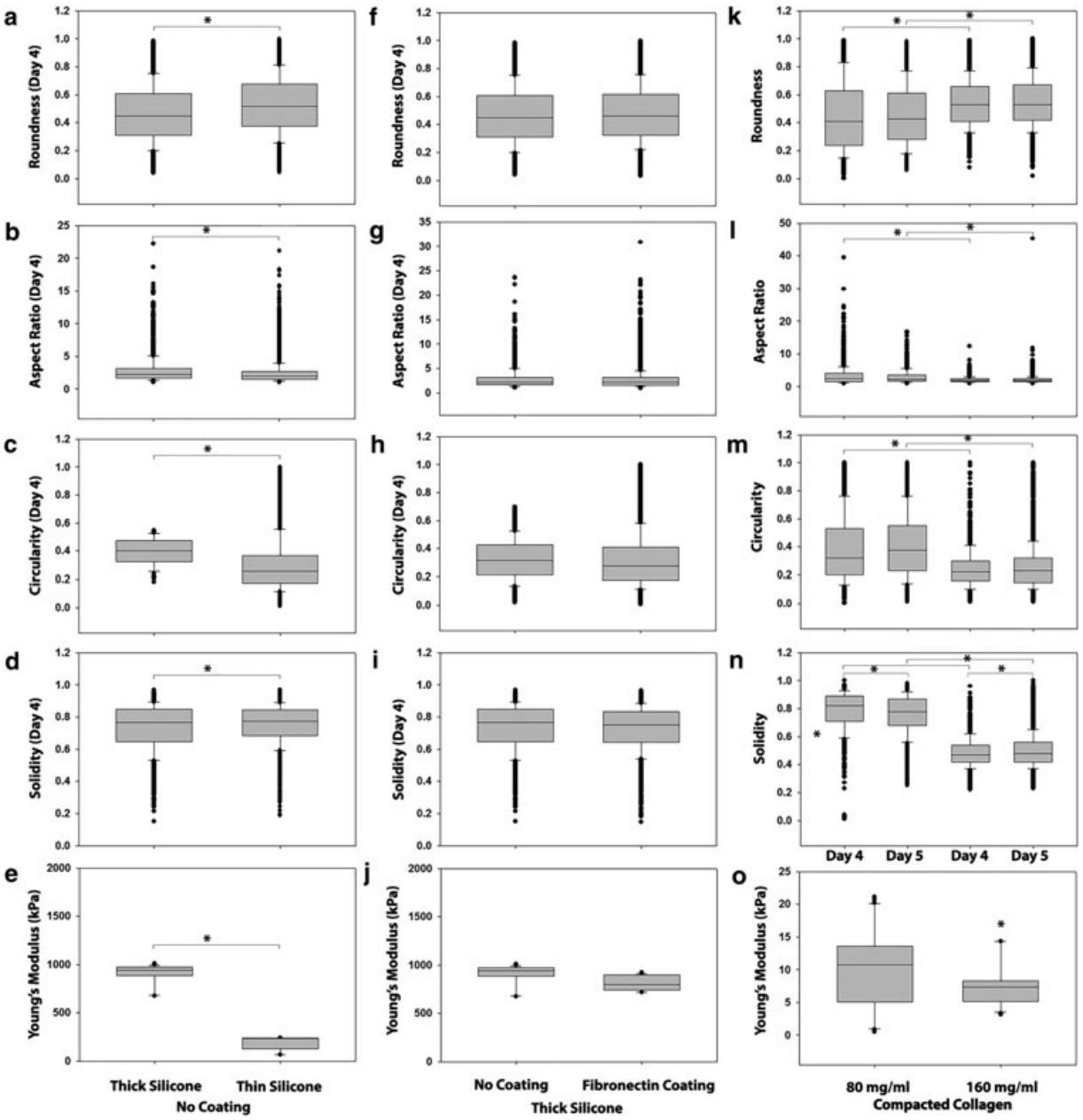

Figure 2. Mesenchymal stem cell (MSC) shape descriptors and nanoscale surface stiffness of thick and thin silicone sheets, thick silicone sheets coated with fibronectin, and 80 mg/ml and 160 mg/ml compacted collagen sheets. This figure reports the shape descriptors roundness (a,f,k), aspect ratio (b,g,l), circularity (c,h,m), and solidity (d,i,n) of calcein-stained MSCs that adhered to the selected biomaterial surfaces (a–d, thick/thin silicone: f–i, thick uncoated/fibronectin-coated silicone; k–n, 80 mg/ml and 160 mg/ml compacted collagen type I on days 4 and 5, and (e,j,o) the nanoscale stiffness of these surfaces measured with atomic force microscopy. The figure illustrates significant differences in all four shape descriptors of MSCs adhering to thick vs. thin silicone sheets ($P < 0.001$, a–d), and differences in the nanoscale stiffness of the thick vs. thin silicone sheets ($P < 0.001$, e). In strong contrast, the four shape descriptors were not significantly different when comparing thick uncoated silicone sheets vs. thick fibronectin-coated silicone sheets (f–i). In addition, there was no significant difference in the nanoscale stiffness between the uncoated and fibronectin-coated silicone surfaces (j). There were significant differences in the shape descriptors of MSCs adhering to 80 mg/ml vs. 160 mg/ml compacted collagen sheets ($P < 0.001$, k–n) and small but significant differences in the nanoscale stiffness between these sheets (o). The box plots give the median and the 25th and 75th percentiles, the error bars give the 10th and 90th percentiles, and outliers are presented in a light tint. *Significant differences, with $P < 0.05$. Number of individually performed experiments for calculating shape descriptors: $n = 3$ sheets for each condition, $n = 2675$–9056 MSCs per condition (silicone) and $n = 1290$–6209 MSCs per condition (compacted collagen). Number of individually performed experiments for AFM: $n = 3$ sheets for each biomaterial category, $n = 9$ different measurement points per sheet

changes. Although differences in solidity were significant, they were relatively small. To correlate MSC shape descriptors with the nanoscale stiffness of the compacted collagen sheets, their Young's modulus was calculated. The Young's modulus of 80 mg/ml compacted collagen sheets was 10.2 ± 0.8 kPa and significantly higher than the Young's modulus of 160 mg/ml sheets ($P < 0.001$), which was 7.2 ± 0.6 kPa (Figure 2o). As shown above for silicone sheets (Figure 2a–e), these data indicated that lower roundness, higher aspect ratio and circularity, and a lower solidity were associated with a higher nanoscale stiffness of the same biomaterial type, presented here for compacted collagen sheets (Figure 2k–o).

3.3. Effects of cyclic stretch on MSC shape descriptors

To assess the effects of tensile forces on MSC shape descriptors, cyclic stretch was applied to MSCs that adhered to compacted collagen sheets with a concentration of

DOI: 10.1002/term

80 mg/ml. This was also performed to assess whether the application of tensile forces results in MSC elongation during cyclic stretch, and whether the effects on elongation are diminished upon cessation of stretch. With both loading regimes (2.5% and 5% strain amplitudes) and after a recovery period of 1 h, cyclic stretch had significant effects on all four shape descriptors (Figure 3a–d). The most obvious changes were that cyclic stretch significantly increased roundness (Figure 3a), decreased aspect ratio (Figure 3b), and increased circularity and solidity ($P < 0.001$; Figure 3c–d), when comparing non-stretched controls with cyclically stretched MSCs. Statistically, all differences between controls vs. 2.5% and controls vs. 5% stretched MSCs and between day 4 vs. day 5 reached significant levels for all four shape descriptors ($P < 0.001$). The effects of time on non-stretched and cyclically stretched MSCs were significantly different for all four shape descriptors ($P < 0.001$; Figure 3a–d). The stretch-induced increase in roundness on day 4 was diminished on day 5 (Figure 3a) and the stretch-induced decrease in aspect ratio on day 4 was also diminished on day 5 (Figure 3b). However, the stretch-induced increase in circularity was further increased (Figure 3c) whereas stretch-induced responses in solidity depended on the strain amplitude (Figure 3d). Thus, cyclic stretch had differential effects over time on roundness and aspect ratio vs. circularity. The non-stretched control MSCs also underwent significant changes in their cellular roundness, aspect ratio, circularity and solidity when comparing days 4 and 5 ($P < 0.001$). However, the changes observed over time in the non-stretched control MSCs were much smaller than the changes that were biomechanically induced. Collectively, these data demonstrated that biomechanical stretch of 2.5% and 5% was associated with a significant change in MSC morphology and, notably, with a rounder MSC morphology (higher roundness, lower aspect ratio) with a smaller amount of membrane protrusions (higher circularity and solidity).

3.4. Changes in MSC shape descriptors after cessation of cyclic stretch

To demonstrate that stretching the biomaterial actually stretched the adhering cells, MSC-seeded compacted collagen sheets were manually stretched on top of a microscope slide, and the calcein-stained, unfixed MSCs were imaged (Figure 4). Non-stretched control MSCs had an aspect ratio of 3.19 and a roundness of 0.398 ± 0.002 (Figure 4b,f). During cyclic stretch, the aspect ratio increased significantly to 3.34 ($P < 0.001$) and roundness decreased significantly to 0.391 ± 0.002 ($P < 0.001$; Figure 4c,f). Thus, cyclic stretch increased aspect ratio (by 4.58%) and decreased MSC roundness (by 1.82%), which is consistent with the idea that elongated MSCs were produced during stretch ($P < 0.001$). On day 4, 1 h after the completion of cyclic stretch, the MSC roundness was significantly increased to 0.438 ± 0.001

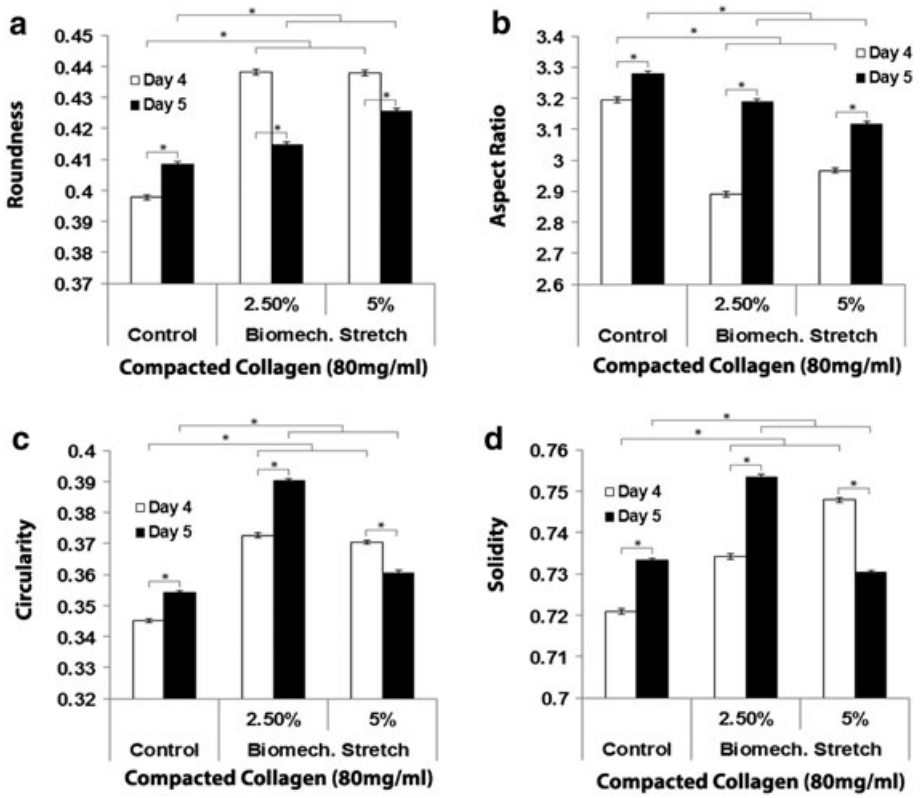

Figure 3. Shape descriptors of mesenchymal stem cells (MSCs) adhering to cyclically stretched 80 mg/ml compacted collagen sheets. This figure illustrates significant differences in the shape descriptors roundness (a), aspect ratio (b), circularity (c), and solidity (d) when comparing cyclically stretched vs. non-stretched control MSCs ($P < 0.001$). The box plots give the median and the 25th and 75th percentiles, the error bars give the 10th and 90th percentiles, and outliers are shown in light tint. *Significant differences, with $P < 0.05$. Number of individually performed experiments for cyclic stretch: $n = 13$ sheets for each loading regime, $n = 44\,444$–$60\,594$ MSCs for each loading regime

DOI: 10.1002/term

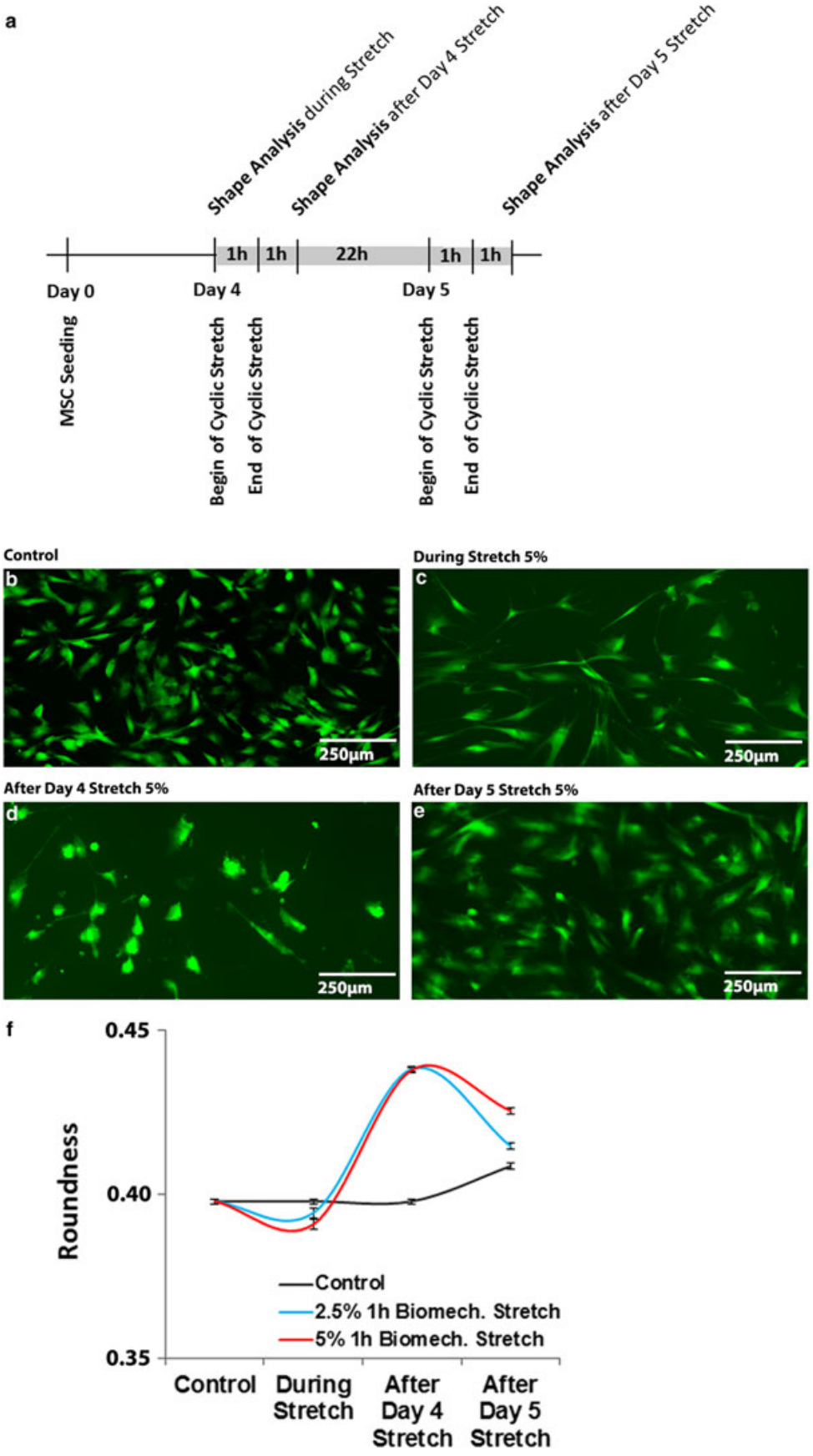

Figure 4. Experimental timeline and changes in mesenchymal stem cell (MSC) shape descriptors after cessation of cyclic stretch. (a) The experimental timeline for cyclic stretch and subsequent analyses. Using representative images of calcein-stained MSCs in a top-down view on the surface of compacted collagen type I sheets, this figure illustrates the roundness values of non-stretched control MSCs (b), of MSCs during static stretch (c), 1 h after cessation of a 5% cyclic stretch on day 4 (d) and 1 h after cessation of a 5% cyclic stretch on day 5 (e). (f) Average roundness and standard errors at these time-points (5% stretch amplitude: red line, 2.5 % amplitude: blue line). Data in (f) is presented as mean ± SEM. Number of individually performed experiments: n = 13 for controls and n = 14 for days 4 and 5 cyclic stretch; n = 5 for values recorded during stretch. [Colour figure can be viewed at wileyonlinelibrary.com]

DOI: 10.1002/term

($P < 0.001$; Figure 4d, f). Interestingly, this suggested that MSCs were rounder after cessation of stretch than during stretch. This was an unexpected observation, which indicated that biomechanically applied elongation of MSCs had led to rounder MSCs. Comparable findings were observed on day 5: 1 h after the completion of cyclic stretch, the roundness was 0.425 ± 0.001 and significantly greater than during stretch ($P < 0.001$) but a little lower than on day 4 ($P < 0.001$; Figure e,f). Under the chosen conditions and with both amplitudes, cyclic stretch led to elongated MSCs during stretch but yielded rounder MSCs after the cessation of stretch; MSCs reverted to their original biomaterial–dictated shape. Collectively, this suggested that the effects of dynamically applied biomechanical forces overpowered the biomaterial-dictated static effects on shape, but only transiently.

3.5. Effects of cyclic stretch on MSC gene expression of SMC markers

To determine the effects of tensile forces on the gene expression of SMC markers, 2.5% and 5% cyclic stretch was applied to compacted collagen sheets (80 mg/ml) and the adhering MSCs. These were subsequently analysed by qRT-PCR. Compared with non-stretched controls, 5% cyclic stretch significantly increased the gene expression of *ACTA2* on day 5 (1.49 ± 0.14-fold, $P < 0.05$; Figure 5a), the expression of *TAGLN* on day 5 (1.22 ± 0.11, 1.71 ± 0.14, $P < 0.05$; Figure 5b) and the expression of *CNN1* on day 4 (1.93 ± 0.45, $P < 0.05$, Figure 5c). In contrast, a 2.5% cyclic stretch only significantly increased the expression of *TAGLN* on day 5. Thus, biomechanical stimulation via a 5% cyclic stretch for 1 h for two consecutive days (on day 4 and day 5) induced the increased expression of the SMC marker genes *ACTA2*, *TAGLN* and *CNN1*. These changes in the gene expression of SMC markers were confirmed on protein level (see the Supplementary material online).

3.6. Biomechanical stimulation did not change MSC numbers

To assess whether biomechanical stimulation had any effects on proliferation, the total number of MSCs that adhered to compacted collagen sheets was calculated. However, the MSC numbers per normalized area did not significantly change when comparing day 4 and day 5 controls, and when comparing cyclically stretched MSCs with controls, regardless of stretch duration or amplitude (see the Supplementary material online). Thus, biomechanical stimulation had no effect on MSC numbers.

3.7. Correlations between biomechanically induced MSC shapes and SMC marker gene expression

Next, a correlation analysis was performed to determine if the biomechanically induced MSC shape descriptors correlated with the expression of specific SMC marker genes. The expression of *ACTA2* correlated significantly with roundness ($P < 0.01$, correlation coefficient 0.309; Figure 6a) and aspect ratio ($P < 0.01$, correlation coefficient –0.357; Figure 6b). The expression of *TAGLN* correlated significantly with solidity ($P < 0.05$, correlation coefficient –0.223; Figure 6c), and the expression of *CNN1* correlated significantly with roundness ($P < 0.01$, correlation coefficient 0.328; Figure 6d), aspect ratio

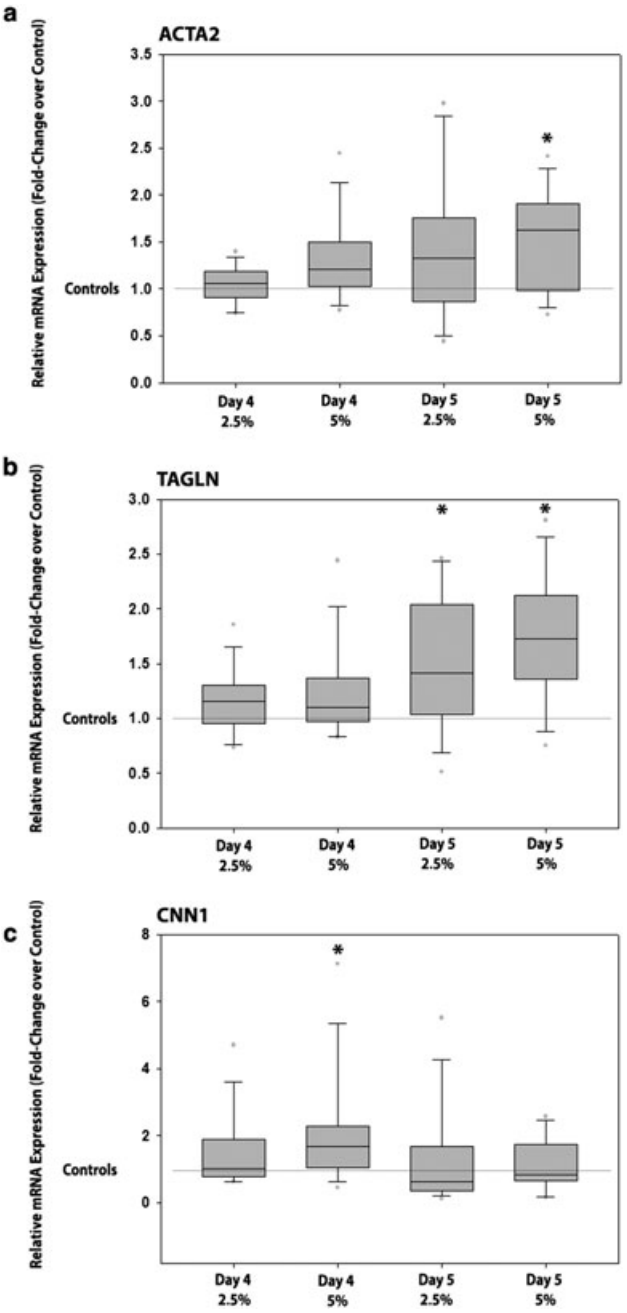

Figure 5. Biomechanically induced changes in gene expression of smooth muscle cell (SMC) markers. This figure reports the gene expression levels (relative mRNA expression) of (a) *ACTA2*, (b) *TAGLN* and (c) *CNN1* of cyclically stretched MSCs, normalized to unstimulated control MSCs (data is presented in fold-change; a value of 1 represents the gene expression level of unstimulated controls for days 4 and 5). Cyclic stretch was performed with 2.5 % and strain 5 % amplitude for 1 h per day on days 4 and 5 at a frequency of 1 Hz. The 80 mg/ml compacted collagen sheets were stretched together with the adhering MSCs, seeding at a density of 5000 MSCs/cm^2. The box plots give the median and the 25th and 75th percentiles, the error bars give the 10th and 90th percentiles, and outliers are shown in a light tint. *Significant differences with $P < 0.05$. The number of individually performed experiments was 13 for each condition

DOI: 10.1002/term

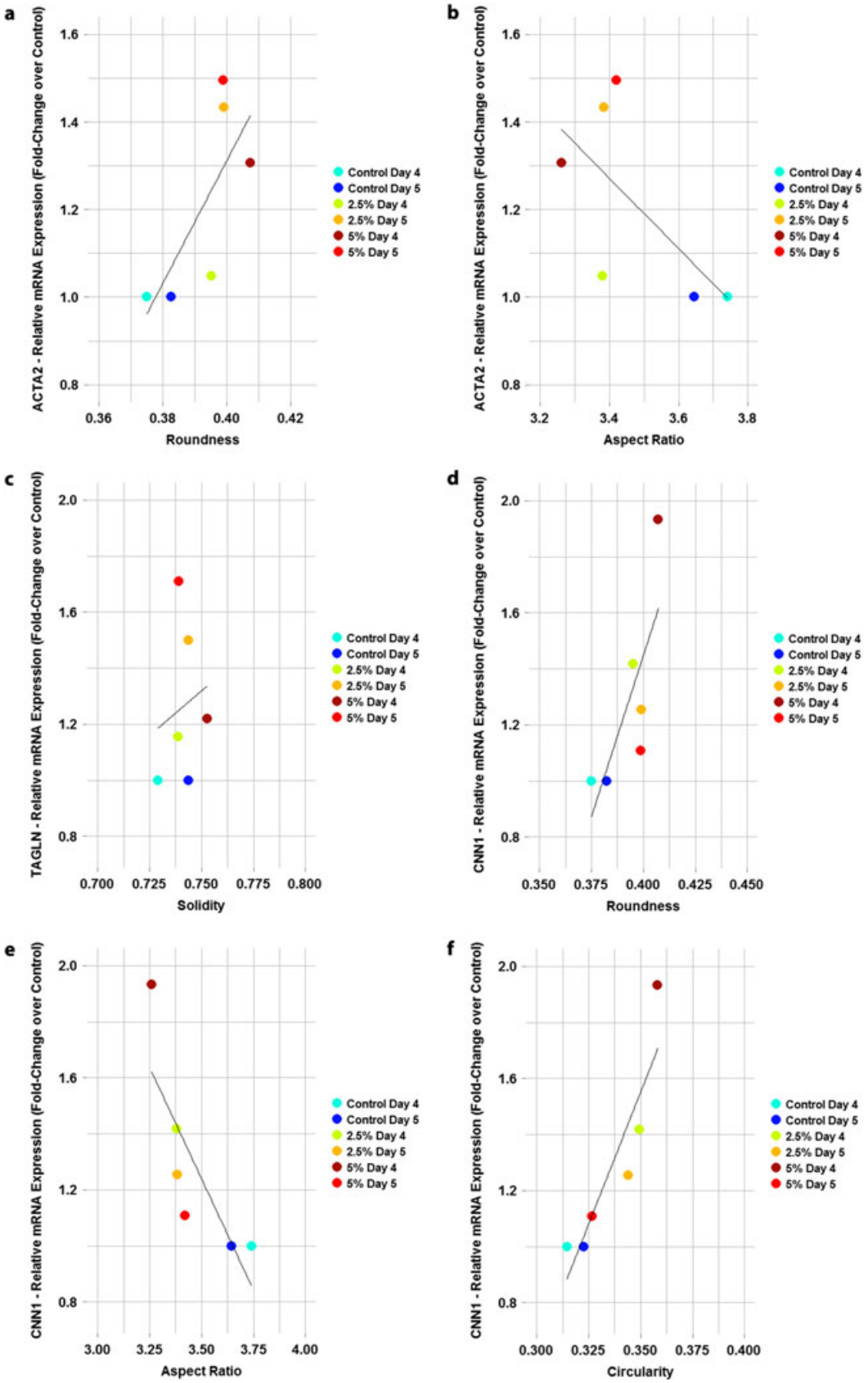

Figure 6. Correlations between biomechanically induced changes in mesenchymal stem cell (MSC) shape descriptors and gene expression levels of SMC markers. On the *x*-axis, this figure reports the shape descriptor values of MSCs for unstimulated controls and 2.5% and 5% cyclically stretched MSCs. On the *y*-axis, this figure reports the gene expression levels of (a,b) *ACTA2*, (c) *TAGLN* and (d–f) *CNN1* of biomechanically stimulated MSCs normalized to unstimulated controls (controls, $n = 1$). Only correlations between shape descriptors and gene expression levels that reached significant levels are presented. Each panel also gives the calculated linear regression line between MSC morphology and gene expression. A single data point represents the average of $n = 13$ individual experiments on the *x*-axis. For each individual experiment, all four shape descriptors were calculated for each individual cell that was recorded (day 4, control $n = 60\,385$ MSCs; day 4, 2.5% stretch $n = 50\,721$ MSCs; day 4, 5% stretch $n = 60\,329$ MSCs; day 5, control $n = 60\,594$ MSCs; day 5, 2.5% stretch $n = 44\,444$ MSCs, day 5, 5% stretch $n = 49\,623$ MSCs). On the *y*-axis, a single data point represents the average mRNA expression of all adherent MSCs, assessed by quantitative reverse-transcription polymerase chain reaction for each individual experiment ($n = 13$). [Colour figure can be viewed at wileyonlinelibrary.com]

DOI: 10.1002/term

Table 1. Changes in shape descriptors as function of biomaterial type, substrate concentration

			Absolute values				Value relative to 80 mg/ml collagen I sheets (%)†			
		Nanoscale stiffness (kPa)*	Roundness	Aspect ratio	Circularity	Solidity	Roundness	Aspect ratio	Circularity	Solidity
Effects associated with biomaterial type and coating										
Compacted collagen I sheets	80 mg/ml concentration	10.2 ± 0.8	0.398	3.19	0.35	0.72	100.0	100.0	100.0	100.0
Uncoated (thick) silicone sheets	762 μm thickness	903.2 ± 18.8	0.465	2.24	0.32	0.77	116.8	70.04	93.55	**106.1**
Uncoated (thin) silicone sheets	127 μm thickness	185.8 ± 14.2	0.524	2.39	0.30	0.75	**131.8**	74.71	**87.39**	104.6
Silicone sheets (thick) coated with:	Collagen I (PureCol)	782.2 ± 21.5	0.488	2.12	0.49	0.76	122.6	**66.41**	**141.3**	105.1
	Collagen I (Roche)	756.9 ± 19.7	0.462	2.27	0.46	0.74	116.1	70.98	133.8	102.8
	Fibronectin	811.0 ± 14.7	0.476	2.16	0.48	0.75	119.6	67.66	137.9	104.2
	Laminin-511		0.471	2.19	0.47	0.76	118.3	68.60	136.4	106.0
Effects associated with biomechanical stimulation										
During 5% stretch	Collagen I sheets (80 mg/ml)		0.391	3.34	0.34	0.71	**98.18**	**104.6**	97.79	**98.81**
1 h after 2.5% cyclical stretch	Collagen I sheets (80 mg/ml)									
	Day 4		0.438	2.89	0.37	0.73	110.1	90.49	107.9	101.8
	Day 5		0.415	3.19	0.37	0.75	104.3	99.83	107.3	104.5
1 h after 5% cyclical stretch	Collagen I sheets (80 mg/ml)									
	Day 4		0.438	2.97	0.37	0.75	110.0	92.89	107.3	103.7
	Day 5		0.425	3.12	0.36	0.73	106.9	97.57	104.4	101.3
Effects of substrate concentration, thickness, and culture time							Value relative to cursive condition (%)			
Effects of substrate concentration (160 mg/ml relative to 80 mg/ml collagen I, on day 4)							**120.8**	**34.95**	**63.87**	**61.96**
Effects of substrate thickness (thin relative to thick silicone, on day 4)							112.8	106.7	93.41	98.60
Effects of time on 80 mg/ml collagen I sheets (day 5 relative to day 4)							101.1	50.45	**107.3**	96.67
Effects of time on 160 mg/ml collagen I sheets (day 5 relative to day 4)							101.0	100.2	104.4	**103.8**
Effects of cyclic stretch amplitude and loading time										
Effects of cyclic stretch amplitude on 80 mg/ml collagen I sheets (5% relative to 2.5%, on day 4)							99.93	102.7	104.7	101.9
Effects of cyclic stretch amplitude on 80 mg/ml collagen I sheets (5% relative to 2.5%, on day 5)							102.5	97.74	97.33	96.93
Effects of cyclic stretch time on 80 mg/ml collagen I sheets (day 5 relative to day 4 at 2.5% amplitude)							**94.71**	**110.3**	99.41	102.6
Effects of cyclic stretch time on 80 mg/ml collagen I sheets (day 5 relative to day 4, at 5% amplitude)							97.15	105.0	92.42	97.65

*Nanoscale stiffness of compressed collagen sheets determined by atomic force microscopy (AFM) was in part reported (Rothdiener et al., 2016).
†Green indicates relative increases, red relative decreases; maxima are in bold. For all given absolute values, the SEM was in the range of ±0.010 to ±0.001.

($P < 0.001$, correlation coefficient –0.376; Figure 6e), and circularity ($P < 0.001$, correlation coefficient 0.408; Figure 6f). Increases in roundness and decreases in aspect ratio always correlated significantly with higher gene expression levels, and those were exclusively observed in the biomechanically stimulated MSCs. Increases in solidity and circularity correlated significantly with higher gene expression levels, which were only observed in the biomechanically stimulated MSCs. Correlations between *ACTA2* expression and circularity ($P = 0.086$) or *TAGLN* expression and roundness ($P = 0.064$) and aspect ratio ($p = 0.051$) showed trends but did not significantly correlate. Thus, biomechanically induced shape changes correlated significantly with changes in gene expression of specific SMC marker genes.

3.8. Relative shape descriptor changes as function of biomaterial type, concentration, application of cyclic stretch and time

Table 1 presents absolute and relative values for the shape descriptors calculated. This allowed comparison of the effects on MSC shape across the various experimental conditions. Colour coding was used, where red indicated relative decreases and green indicated relative increases. Biomaterial type, coating, concentration as well as culture time and the amplitude and loading time of cyclic stretch had all complex effects on MSC shape. However, the strength of the effects varied considerably.

4. Discussion

The present study demonstrates that both biomaterial and biomechanical cues determine MSC morphology measured via quantitative shape descriptors. First, it was demonstrated that specific MSC baseline morphologies were associated with the nanoscale stiffness of the biomaterial surface to which the MSCs adhered. This is important because it implies that specific baseline shapes can be generated by choosing different biomaterial properties. Next, when applying cyclic tensional forces, time- and amplitude-dependent effects on MSC shape were revealed and, as was expected, demonstrated that MSC elongation occurred during cyclic stretch. Surprisingly, after cessation of stretch MSC shape did not remain elongated; instead a significantly rounder cellular shape was observed. This suggested a remodelling effect of MSC shape in response to tensile forces, which has not been previously described. Finally, it was asked whether dynamic cues on cellular shape can potentially overpower static cues, or vice versa. To answer this question, a system of two competing cues was used, with dynamic effects on MSC shape through cyclic stretch and static effects on shape through the stiffness-defined biomaterial. This approach demonstrated that the effects of dynamically applied biomechanical forces on cellular shape can overpower the biomaterial-dictated static effects on shape, but only transiently. Ultimately, MSC shape reverts towards its original biomaterial-dictated state. The insights gained in the present study broaden our methodology for measuring and understanding MSC shape under static and dynamic conditions. This will be helpful for designing the next generation of scaffolds aimed at directing MSC behaviour under mechanical load *in situ*.

As *ex vivo* MSC culturing performed on rigid tissue culture plastics may adversely affect the multipotency of MSCs (Zhang and Kilian, 2013), appropriate biomaterials with lineage-specific biophysical cues may serve as a starting point to develop cell-based therapies, where endogenous *in vivo* signals can culminate in direct full differentiation (Lee et al., 2014). The first hypothesis of the present study was that specific MSC shapes can be generated as a function of the biomaterials chosen and the nanoscale stiffness associated with these biomaterials. The shape of human bone-marrow derived MSCs that adhered to different biomaterials was compared with those of similar stiffness (uncoated vs. fibronectin-coated silicon sheets), and with similar biomaterial types with different stiffnesses (thin vs. thick silicone sheets, and compacted collagen sheets with 80 mg/ml vs. 160 mg/ml collagen I concentration). Silicone sheets were previously used to investigate MSC behaviour under cyclic stretch (Hamilton et al., 2004; Park et al., 2004; Liu et al., 2008; Maul et al., 2011; Morita et al., 2013; Tondon and Kaunas, 2014). Compacted collagen hydrogels compressed into dense sheets are termed compressed collagen (Brown et al., 2005) and were previously used for the tissue engineering of artificial corneas (Levis et al., 2012) and skin (Braziulis et al., 2012). The present study demonstrated that higher nanoscale stiffness, compared with lower stiffness of the same biomaterial type, was associated with lower MSC roundness, higher aspect ratio and circularity, and a lower solidity. In strong contrast, similar nanoscale stiffnesses of different biomaterials were associated with statistically comparable MSC shape descriptors. These data strongly suggested that nanoscale stiffness has a significant effect on MSC shape descriptors. This implied that specific shapes can be generated by choosing specific nanoscale stiffnesses for MSC adherence. Other parameters such as fibre type and diameter of a given biomaterial also affect MSC morphology and, specifically, roundness (Phipps et al., 2011). Thus, when comparing different biomaterial types with different nanoscale stiffnesses, a more complex situation would arise. This topic warrants further study. However, nanoscale stiffness is clearly a relevant biomaterial property for generating specific shapes of MSCs quantified with shape descriptors just as the present study demonstrates.

As demonstrated by the present study shape descriptors can be used for describing MSC morphology in a quantitative fashion. In two recent publications, shape descriptors were successfully used for characterizing cellular shape in analyses pertaining to the differentiation of MSC into osteoblasts (Rocca et al., 2015) and to acute brain injury models in mice (Zanier et al., 2015). The descriptors roundness and aspect ratio are somewhat intuitive. A high roundness describes a rounder shape, whereas a high

DOI: 10.1002/term

aspect ratio describes an elliptical shape (Figure 1). These have shown to be relevant factors as rounded MSC shapes can aid adipogenic differentiation, while elongated shapes can aid myogenesis (Yang et al., 1999; Hamilton et al., 2004; Nieponice et al., 2007; Maul et al., 2011) and osteogenic differentiation (McBeath et al., 2004). Circularity and solidity can be understood best in terms of membrane protrusions such as lamellipodia (broad, flat protrusions at the leading edge of cells), filopodia (finger-like protrusions) and blebs (outward bulges in the plasma membrane) that are relevant for adhesion, migration and rigidity sensing (Krause and Gautreau, 2014). High values for circularity and solidity indicate fewer such protrusions. Specifically, it appears that circularity may be a better indication of the presence of filopodia as it would decrease significantly as the number of small protrusions increases. These small protuberances radically increase the perimeter, which increases geometrically in the circularity measurement. Blebbing would have a less prominent effect on circularity but would greatly reduce solidity as the larger part of the cell is a concave area. These associations need to be confirmed in future studies. The present study demonstrated that the chosen methodology pertaining to shape analysis was successful in identifying differences in MSC shape across the experimental conditions tested. This was, in part, due to the semi-automated approach and a large number of data points (cells analysed) that were acquired (44 444–60 594 MSCs) per condition. Another question raised by the data pertains to the apparently relatively small amount(s) of the induced changes in MSC morphology. For example, a 5% stretch led to a maximum change of 10% in roundness and 7% in aspect ratio, whereas biomaterial-associated changes in shape induced a change of 20% in roundness and of 34% in aspect ratio. To demonstrate the relevance of these relatively small amounts in the context of the literature, geometrically defined micro-engineered adhesion sites used in Kilian *et al.* (2010) were analyzed. That study used rounded pentagonal geometries for inducing adipogenic and edged pentagonal geometries for inducing osteogenic differentiation of MSCs. A difference of 3% roundness and 3% aspect ratio between the two shape types was calculated, illustrating, together with the present study, that small changes in MSC morphology can have a large impact.

Next, cyclic stretch-induced changes in MSC shape were examined. The underlying hypothesis was that tensile forces may result in MSC elongation during cyclic stretch, but this is relieved upon cessation of stretch, as a consequence of diminished external force input. *In vivo*, the mechanical environment surrounding the stem cells changes dynamically (Sun et al., 2012), and external biomechanical forces and matrix mechanics are key regulators of stem cell fate (Engler et al., 2006; Sun et al., 2012). In this context, cyclic tensile forces have been used successfully for the stimulation of tenogenesis (Wang et al., 2013), myogenesis (Maul et al., 2011), osteogenesis (Jagodzinski et al., 2004), and chondrogenesis of the intervertebral disk (Driscoll et al., 2013) and articular cartilage (McMahon et al., 2008). The data from the present study demonstrated that cyclic stretch of MSCs induced significant cell elongation during stretch that was comparable to the stretch applied to the underlying biomaterial, which supports previous data (Maul et al., 2011). However, not much attention has been given to cell shapes after biomechanical stimulation. Usually, the experimental design of studies deploying cyclic stretch consists of measuring cells immediately upon completion of stimulation (Hamilton et al., 2004; Park et al., 2004; Kurpinski et al., 2006, 2009; Nieponice et al., 2007; O'Cearbhaill et al., 2008; Zhang et al., 2008; Ghazanfari et al., 2009; Maul et al., 2011; Sarraf et al., 2011; Throm Quinlan et al., 2011) except for a live microscopy study (Tondon and Kaunas, 2014) or studies that assessed the effects on MSC proliferation (Kurpinski et al., 2006; Ghazanfari et al., 2009). Moreover, few studies investigated MSC shape in combination with cyclic stretch (Zhang et al., 2008; Ghazanfari et al., 2009; Maul et al., 2011; Throm Quinlan et al., 2011). It is believed that the present study is the first to investigate MSC shape systematically before, during, and after the completion of cyclic stretch. Finally, the present study attempted to address whether dynamic cues or static cues had more influence over cell shape using a system of two competing cues with dynamic and static effects on MSC shape. Most surprisingly, it was uncovered that cyclic stretch led over time to a rounder MSC shape. This clearly uncovered an unreported and novel idea of shape remodelling during the period immediately following biomechanical stimulation. This behaviour is likely a consequence of diminished force input. It was not associated with proliferation-associated rounding as MSC numbers did not change significantly across the stretch experiment conditions, and because non-adherent MSC would be lost into the medium of the loading chamber. Thus, the data demonstrated that changes in MSC shape occurred during stretch but continued to occur after the completion of stretch, and that stretch had time-dependent effects on roundness and aspect ratio, and amplitude-dependent effects on roundness and circularity. Moreover, the data clearly demonstrated that biomaterial properties dictated MSC shape but this effect was temporarily overruled by cyclic biomechanical loading. Upon relieving cyclic biomechanical tension, MSC shape reverted to the shape associated with the biomaterial. Moreover, the reverting of shape from the stretch-generated values towards the biomaterial-associated shape values caused the shapes to become even rounder, overshooting the initial roundness values seen before stretch. However, the roundness values were approximately similar to non-stretched controls after the second day of stretch. This implies that MSC shape generated during cyclic stretch could potentially be lost after stimulation is stopped, and that this occurs within a relatively short time. It also emphasizes that biomaterials could be designed to sustain or counteract biomechanically induced shapes. Thus, shape-controlling biomechanical forces and biomaterials could theoretically be used for differential or synergistic effects on MSC shape.

Given the range of MSC shapes generated here, the study finally enquired how the recorded shapes may relate to changes in gene expression. This was undertaken in the context of MSCs differentiating towards a SMC phenotype because dynamic elongation of MSCs is a well-recognized model for inducing a SMC phenotype (Hamilton et al., 2004; Nieponice et al., 2007; Maul et al., 2011) and because elongated MSC morphologies are associated with increased expression of smooth muscle markers (Yang et al., 1999; Maul et al., 2011). A recent study uncovered that the attempt to drive differentiation of MSCs with soluble stimulators of smooth muscle differentiation was only successful when the MSCs were physically permitted to elongate (Yang et al., 1999). Thus, MSC elongation seemed relevant for inducing a SMC phenotype in MSCs. We reported in the previous section of the discussion that cyclic stretch led to an elongated MSC shape but that cessation of stretch was associated with complex changes in shape. The resulting shapes and the corresponding expression levels of myogenic marker genes are given in Figure 6. Specific aspects of MSC morphology, quantified with cellular shape descriptors, correlated significantly with the expression levels of specific marker genes. In particular, *ACTA2* correlated with roundness and aspect ratio (Figure 6a,b), *TAGLN* with solidity (Figure 6c), and *CNN1* with roundness, aspect ratio, and circularity (Figure 6d–f). Thus, shape and differentiation were clearly associated under the chosen conditions. Interestingly, lowest roundness, highest aspect ratio and lowest circularity values were associated with lowest gene expression levels, occurring in the non-stretched controls. This is important because the nanoscale stiffness of the 80 mg/ml compacted collagen sheets was ~10 kPa and, thus, in the stiffness range of 8–17 kPa known to support myogenic differentiation of MSCs (Engler et al., 2006). Nevertheless, the non-stretched control MSCs that experienced myogenic differentiation-supporting nanoscale stiffness through the compacted collagen sheets exhibited the lowest expression of SCM marker genes. In contrast, highest roundness, lowest aspect ratio and highest circularity were associated with the highest expression of marker genes and were exclusively observed in the biomechanically stretched groups. This biomechanically induced increase in SMC marker expression was confirmed on protein level (see the Supplementary material online,). One interpretation is that the added effects of tensional force and biomaterial stiffness were more effective in inducing the gene expression of SMC markers in MSCs than stiffness alone. This is supported by Kurpinski *et al.* (2009) who demonstrated that a synergistic upregulation of *CNN1* through TGF-β1 in combination with cyclic stretch was greater than the increase in response to either stimulus alone. In addition, the present study emphasized that specific shape descriptor values were associated (and significantly correlated) with specific marker profiles. For example, a roundness value of approximately 0.4 and an aspect ratio value of 3.4 were critical values for the highest gene expression levels of *ACTA2* and *CNN1*, observed under the chosen conditions. Circularity values higher than 0.35 were critical for a high expression of *CNN1*. Thus, specific shape descriptor values may serve as a future template for the induction of SMC phenotype and may also be adapted for other differentiation lineages. Finally, these data illustrate that even subtle differences in MSC morphology may have a relevant impact on MSC behaviour, and that using quantitative shape descriptors is a suitable method for studying this impact.

5. Conclusion

The present study demonstrates that MSC morphology can be measured using quantitative shape descriptors. The MSC shape was surprisingly dynamic and could be manipulated through different methods. Dynamic tensile forces were more effective in defining MSC shape than stiffness-related cues. However, the biomechanical effects on cellular shape were transient and MSC shape ultimately reverted back to the shape dictated by biomaterial properties. A potential application of this information would be to develop shape-instructive biomaterials that transduce the dynamic *in vivo* biomechanical environment into specific MSC shapes for controlling MSC behaviour.

Acknowledgments

The authors are grateful for the support we received from the German Research Council (RO2511/3-1 to B.R., KL709/13-1 to G.K. and AI16/23-1 to W.K.A.), the German Ministry of Education and Research (BMBF) and the company AESCULAP [01KQ0902B REGiNA TP2 (BR)], which supported acquisition of the Bose ElectroForce 5210 BioDynamic-Test-System, and the intramural financial and personnel support of the BG Trauma Clinic Tübingen (Berufsgenossenschaftliche Unfallklinik Tuebingen) and the clinic operator Heidelberg Association for the Treatment of Occupational Injuries (Verein für Berufsgenossenschaftliche Heilbehandlung Heidelberg e.V.).

Conflict of interest

The authors declare no conflicts of interest.

References

Aicher WK, Buhring HJ, Hart M, *et al*. 2011; Regeneration of cartilage and bone by defined subsets of mesenchymal stromal cells – potential and pitfalls. *Adv Drug Del Rev* **63**: 342–351.

Braziulis E, Diezi M, Biedermann T, *et al*. 2012; Modified plastic compression of collagen hydrogels provides an ideal matrix for clinically applicable skin substitutes. *Tissue Engineering Part C Methods* **18**: 464–474.

Brown RA, Wiseman M, Chuo CB, *et al*. 2005; Ultrarapid engineering of biomimetic materials and tissues: fabrication of nano- and microstructures by plastic compression. *Adv Funct Mater* **15**: 1762–1770.

Bustin SA, Benes V, Garson JA, *et al*. 2009; The MIQE guidelines: minimum information for publication of quantitative real-time PCR experiments. *Clin Chem* **55**: 611–622.
Caplan AI. 2007; Adult mesenchymal stem cells for tissue engineering versus regenerative medicine. *J Cell Physiol* **213**: 341–347.
Dominici M, Le Blanc K, Mueller I, *et al*. 2006; Minimal criteria for defining multipotent mesenchymal stromal cells. The International Society for Cellular Therapy position statement. *Cytotherapy* **8**: 315–317.
Driscoll TP, Nakasone RH, Szczesny SE, *et al*. 2013; Biaxial mechanics and inter-lamellar shearing of stem-cell seeded electrospun angle-ply laminates for annulus fibrosus tissue engineering. *J Orthop Res* **31**: 864–870.
Engler AJ, Sen S, Sweeney HL, *et al*. 2006; Matrix elasticity directs stem cell lineage specification. *Cell* **126**: 677–689.
Felka T, Schafer R, Schewe B, *et al*. 2009; Hypoxia reduces the inhibitory effect of IL-1beta on chondrogenic differentiation of FCS-free expanded MSC. *Osteoarthr Cartil* **17**: 1368–1376.
Folkman J, Moscona A. 1978; Role of cell shape in growth control. *Nature* **273**: 345–349.
Ghazanfari S, Tafazzoli-Shadpour M, Shokrgozar MA. 2009; Effects of cyclic stretch on proliferation of mesenchymal stem cells and their differentiation to smooth muscle cells. *Biochem Biophys Res Commun* **388**: 601–605.
Hamilton DW, Maul TM, Vorp DA. 2004; Characterization of the response of bone marrow-derived progenitor cells to cyclic strain: implications for vascular tissue-engineering applications. *Tissue Eng* **10**: 361–369.
Jagodzinski M, Drescher M, Zeichen J, *et al*. 2004; Effects of cyclic longitudinal mechanical strain and dexamethasone on osteogenic differentiation of human bone marrow stromal cells. *Eur Cells Mater* **7**: 35–41.
Kilian KA, Bugarija B, Lahn BT, *et al*. 2010; Geometric cues for directing the differentiation of mesenchymal stem cells. *Proc Natl Acad Sci U S A* **107**: 4872–4877.
Klein G, Hart ML, Brinchmann JE, *et al*. 2015; Mesenchymal stromal cells for sphincter regeneration. *Adv Drug Del Rev* **82–83**: 123–136.
Krause M, Gautreau A. 2014; Steering cell migration: lamellipodium dynamics and the regulation of directional persistence. *Nature Rev Mol Cell Biol* **15**: 577–590.
Kurpinski K, Chu J, Hashi C, *et al*. 2006; Anisotropic mechanosensing by mesenchymal stem cells. *Proc Natl Acad Sci U S A* **103**: 16095–16100.
Kurpinski K, Chu J, Wang D, *et al*. 2009; Proteomic profiling of mesenchymal stem cell responses to mechanical strain and TGF-beta1. *Cell Mol Bioeng* **2**: 606–614.
Lee J, Abdeen AA, Kilian KA. 2014; Rewiring mesenchymal stem cell lineage specification by switching the biophysical microenvironment. *Sci Rep* **4**: 5188.
Levis HJ, Peh GS, Toh KP, *et al*. 2012; Plastic compressed collagen as a novel carrier for expanded human corneal endothelial cells for transplantation. *PLoS One* **7**: e50993.
Liu B, Qu MJ, Qin KR, *et al*. 2008; Role of cyclic strain frequency in regulating the alignment of vascular smooth muscle cells *in vitro*. *Biophys J* **94**: 1497–1507.
Manasek FJ, Burnside MB, Waterman RE. 1972; Myocardial cell shape change as a mechanism of embryonic heart looping. *Dev Biol* **29**: 349–371.
Maul TM, Chew DW, Nieponice A, *et al*. 2011; Mechanical stimuli differentially control stem cell behavior: morphology, proliferation, and differentiation. *Biomech Model Mechanobiol* **10**: 939–953.
McBeath R, Pirone DM, Nelson CM, *et al*. 2004; Cell shape, cytoskeletal tension, and RhoA regulate stem cell lineage commitment. *Dev Cell* **6**: 483–495.
McMahon LA, Reid AJ, Campbell VA, *et al*. 2008; Regulatory effects of mechanical strain on the chondrogenic differentiation of MSCs in a collagen-GAG scaffold: experimental and computational analysis. *Ann Biomed Eng* **36**: 185–194.
Morita Y, Watanabe S, Ju Y, *et al*. 2013; Determination of optimal cyclic uniaxial stretches for stem cell-to-tenocyte differentiation under a wide range of mechanical stretch conditions by evaluating gene expression and protein synthesis levels. *Acta Bioeng Biomech* **15**: 71–79.
Nieponice A, Maul TM, Cumer JM, *et al*. 2007; Mechanical stimulation induces morphological and phenotypic changes in bone marrow-derived progenitor cells within a three-dimensional fibrin matrix. *J Biomed Mater Res A* **81**: 523–530.
O'Cearbhaill ED, Punchard MA, Murphy M, *et al*. 2008; Response of mesenchymal stem cells to the biomechanical environment of the endothelium on a flexible tubular silicone substrate. *Biomaterials* **29**: 1610–1619.
Park JS, Chu JS, Cheng C, *et al*. 2004; Differential effects of equiaxial and uniaxial strain on mesenchymal stem cells. *Biotechnol Bioeng* **88**: 359–368.
Phipps MC, Clem WC, Catledge SA, *et al*. 2011; Mesenchymal stem cell responses to bone-mimetic electrospun matrices composed of polycaprolactone, collagen I and nanoparticulate hydroxyapatite. *PLoS One* **6**: e16813.
Pilz GA, Ulrich C, Ruh M, *et al*. 2011; Human term placenta-derived mesenchymal stromal cells are less prone to osteogenic differentiation than bone marrow-derived mesenchymal stromal cells. *Stem Cell Dev* **20**: 635–646.
Rocca A, Marino A, Rocca V, *et al*. 2015; Barium titanate nanoparticles and hypergravity stimulation improve differentiation of mesenchymal stem cells into osteoblasts. *Int J Nanomedicine* **10**: 433–445.
Rolauffs B, Williams JM, Aurich M, *et al*. 2010; Proliferative remodeling of the spatial organization of human superficial chondrocytes distant from focal early osteoarthritis. *Arthritis Rheum* **62**: 489–498.
Rolauffs B, Rothdiener M, Bahrs C, *et al*. 2011; Onset of preclinical osteoarthritis: the angular spatial organization permits early diagnosis. *Arthritis Rheum* **63**: 1637–1647.
Rothdiener M, Hegemann M, Uynuk-Ool T, *et al*. 2016; Stretching human mesenchymal stromal cells on stiffness-customized collagen type I generates a smooth muscle marker profile without growth factor addition. *Sci Rep* **6**: 35840.
Sarraf CE, Otto WR, Eastwood M. 2011; *In vitro* mesenchymal stem cell differentiation after mechanical stimulation. *Cell Prolif* **44**: 99–108.
Singhvi R, Kumar A, Lopez GP, *et al*. 1994; Engineering cell shape and function. *Science* **264**: 696–698.
Sun Y, Chen CS, Fu J. 2012; Forcing stem cells to behave: a biophysical perspective of the cellular microenvironment. *Ann Rev Biophys* **41**: 519–542.
Throm Quinlan AM, Sierad LN, Capulli AK, *et al*. 2011; Combining dynamic stretch and tunable stiffness to probe cell mechanobiology *in vitro*. *PLoS One* **6**: e23272.
Tondon A, Kaunas R. 2014; The direction of stretch-induced cell and stress fiber orientation depends on collagen matrix stress. *PLoS One* **9**: e89592.
Ulrich C, Rolauffs B, Abele H, *et al*. 2013; Low osteogenic differentiation potential of placenta-derived mesenchymal stromal cells correlates with low expression of the transcription factors Runx2 and Twist2. *Stem Cells Dev* **22**: 2859–2872.
Wang W, Deng D, Li J, *et al*. 2013; Elongated cell morphology and uniaxial mechanical stretch contribute to physical attributes of niche environment for MSC tenogenic differentiation. *Cell Biol Int* **37**: 755–760.
Yang Y, Relan NK, Przywara DA, Schuger L. 1999; Embryonic mesenchymal cells share the potential for smooth muscle differentiation: myogenesis is controlled by the cell's shape. *Development* **126**: 3027–3033.
Zanier ER, Fumagalli S, Perego C, *et al*. 2015; Shape descriptors of the 'never resting' microglia in three different acute brain injury models in mice. *Intensive Care Med Exp* **3**: 39.
Zhang D, Kilian KA. 2013; The effect of mesenchymal stem cell shape on the maintenance of multipotency. *Biomaterials* **34**: 3962–3969.
Zhang L, Kahn CJ, Chen HQ, *et al*. 2008; Effect of uniaxial stretching on rat bone mesenchymal stem cell: orientation and expressions of collagen types I and III and tenascin-C. *Cell Biol Int* **32**: 344–352.

Supporting information

Additional supporting information may be found in the online version of this article at the publisher's web-site.